JACS
JOURNAL OF THE AMERICAN CHEMICAL SOCIETY
Article
pubs.acs.org/JACS

Synthesis of Graphene Nanoribbons by Ambient-Pressure Chemical Vapor Deposition and Device Integration

Zongping Chen,[†] Wen Zhang,[†] Carlos-Andres Palma,[§] Alberto Lodi Rizzini,[∥,⊥] Bilu Liu,[#] Ahmad Abbas,[#,⊗] Nils Richter,[▽,¶] Leonardo Martini,[∥,⊥] Xiao-Ye Wang,[†] Nicola Cavani,[∥,⊥] Hao Lu,[†] Neeraj Mishra,[×] Camilla Coletti,[×] Reinhard Berger,[‡] Florian Klappenberger,[§] Mathias Kläui,[▽,¶] Andrea Candini,[⊥] Marco Affronte,[∥,⊥] Chongwu Zhou,[#] Valentina De Renzi,[∥,⊥] Umberto del Pennino,[∥,⊥] Johannes V. Barth,[§] Hans Joachim Räder,[†] Akimitsu Narita,[†] Xinliang Feng,*[,‡] and Klaus Müllen*[,†]

[†]Max Planck Institute for Polymer Research, Ackermannweg 10, D-55128 Mainz, Germany

[‡]Center for Advancing Electronics Dresden and Department of Chemistry and Food Chemistry, Technische Universität Dresden, Mommsenstraße 4, D-01062 Dresden, Germany

[§]Physik-Department, Technische Universität München, James-Franck-Straße 1, D-85748 Garching, Germany

[∥]Dipartimento di Scienze Fisiche, Informatiche e Matematiche, Università di Modena e Reggio Emilia, I-41125 Modena, Italy

[⊥]CNR-NANO, Istituto Nanoscienze, Centro S3, I-41125 Modena, Italy

[#]Department of Electrical Engineering and Department of Chemistry, University of Southern California, Los Angeles, California 90089, United States

[⊗]Department of Electrical Engineering, King Abdulaziz University, Abdullah Sulayman Street, Jeddah 22254, Saudi Arabia

[▽]Institut für Physik, Johannes Gutenberg Universität-Mainz, Staudingerweg 7, D-55128 Mainz, Germany

[¶]Graduate School of Excellence Materials Science in Mainz, Johannes Gutenberg Universität-Mainz, Staudingerweg 9, D-55128 Mainz, Germany

[×]Center for Nanotechnology Innovation @ NEST, Istituto Italiano di Tecnologia, Piazza San Silvestro 12, 56127 Pisa, Italy

Supporting Information

ABSTRACT: Graphene nanoribbons (GNRs), quasi-one-dimensional graphene strips, have shown great potential for nanoscale electronics, optoelectronics, and photonics. Atomically precise GNRs can be "bottom-up" synthesized by surface-assisted assembly of molecular building blocks under ultra-high-vacuum conditions. However, large-scale and efficient synthesis of such GNRs at low cost remains a significant challenge. Here we report an efficient "bottom-up" chemical vapor deposition (CVD) process for inexpensive and high-throughput growth of structurally defined GNRs with varying structures under ambient-pressure conditions. The high quality of our CVD-grown GNRs is validated by a combination of different spectroscopic and microscopic characterizations. Facile, large-area transfer of GNRs onto insulating substrates and subsequent device fabrication demonstrate their promising potential as semiconducting materials, exhibiting high current on/off ratios up to 6000 in field-effect transistor devices. This value is 3 orders of magnitude higher than values reported so far for other thin-film transistors of structurally defined GNRs. Notably, on-surface mass spectrometry analyses of polymer precursors provide unprecedented evidence for the chemical structures of the resulting GNRs, especially the heteroatom doping and heterojunctions. These results pave the way toward the scalable and controllable growth of GNRs for future applications.

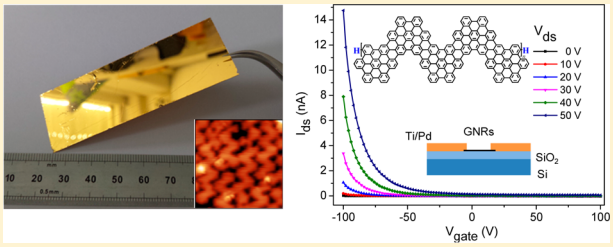

INTRODUCTION

Graphene is a two-dimensional semimetallic crystal with zero bandgap,[1−3] which hinders its use in many electronic and optoelectronic devices, where a suitable bandgap is essential.[4,5] It has been predicted by theoretical studies that narrow (<10 nm) graphene nanoribbons (GNRs) with armchair-type edges exhibit semiconducting behavior, due to the intense quantum confinement and edge effects.[6−8] Whereas the predominant "top-down" approaches, such as lithographical patterning of graphene[9,10] and unzipping of carbon nanotubes,[11,12] can hardly control the width and edge structure of GNRs, surface-assisted[13−15] and solution-mediated[16−20] "bottom-up" methods have been developed to synthesize atomically precise GNRs. Such "bottom-up"-synthesized ultra-narrow (∼1−2 nm) GNRs have demonstrated large bandgaps of ∼1−2 eV with visible to

Received: October 4, 2016
Published: November 4, 2016

ACS Publications © 2016 American Chemical Society

DOI: 10.1021/jacs.6b10374
J. Am. Chem. Soc. 2016, 138, 15488−15496

near-infrared (NIR) absorption,[16−23] rendering them highly interesting for a broad range of applications in next-generation transistors, as well as optoelectronic and photonic devices.[24−26] However, the device applications of the "bottom-up"-synthesized GNRs are still elusive. One reason is that the processing of solution-synthesized GNRs is a major obstacle due to their limited solubility and tendency to aggregate in dispersions.[17,19,20,27] On the other hand, the amount of GNRs accessible by surface-assisted methods is limited, and the elaborate and costly ultra-high-vacuum (UHV) equipment restricts the large-scale fabrication and further use of the GNRs. Sakaguchi and Nakae et al. have previously proposed the use of chemical vapor deposition (CVD) for the on-surface synthesis of GNRs, but low pressure was required for the process, and unambiguous elucidation of the quality and precise structures of the resulting GNRs has remained elusive.[28]

The precise structures of the GNRs "bottom-up" synthesized under UHV have been demonstrated by high-resolution scanning probe microscopy (SPM) together with various spectroscopic characterizations, including Raman spectroscopy and X-ray photoelectron spectroscopy (XPS).[13,14,29−32] Nevertheless, there is still often a lack of direct evidence for the precise chemical structures of the GNRs. For example, C and N atoms cannot be directly distinguished in GNRs because of their nearly identical topographic morphology.[14,31] To date, there is thus no direct evidence for the precise chemical composition of heteroatom-doped GNRs and their heterojunctions.[14,30,31,33]

Here, we demonstrate an efficient ambient-pressure CVD process for inexpensive and high-throughput growth of structurally defined GNRs over large areas, employing hydrogen gas as oxygen scavenger. The GNRs formed by this CVD method exhibit structural quality and properties comparable with those of the same GNRs synthesized under UHV conditions, as supported by Raman spectroscopy, XPS, high-resolution electron energy loss spectroscopy (HREELS), and scanning tunneling microscopy (STM) characterizations. Homogenous GNR films over areas of square centimeters can be obtained and successfully transferred to nonconducting wafers, allowing for facile device integration. Thus-fabricated field-effect transistor (FET) devices exhibit a large current on/off ratio of up to 6000, which is significantly higher than values reported so far for thin-film transistors made with structurally defined GNRs.[27,28,34] Moreover, by using graphene electrodes, the contact resistance can be drastically reduced while preserving the high current on/off ratio. This "bottom-up" CVD method further allows the growth of N-doped and N,S-co-doped GNRs as well as their heterojunctions, demonstrating the versatility and scalability of this process, which provides access to a broad class of GNRs with engineered structures and properties based on molecular-scale design. Importantly, high-resolution mass spectrometry (MS) analyses of their early-stage polyphenylene precursors provided strong evidence for the chemical composition at the termini as well as the doping and heterostructures of the CVD-grown GNRs.

RESULTS AND DISCUSSION

CVD Growth of GNRs. For the growth of chevron-type GNRs, the halogen-functionalized monomer 6,11-dibromo-1,2,3,4-tetraphenyltriphenylene (**DBTT**) was used as molecular precursor (Figures 1 and S1). In a CVD setup, the **DBTT** molecules were sublimed by a heating belt and deposited on a Au/mica surface that was kept in the central zone of a horizontal tube furnace at a temperature of 250 °C (Figures 1a and S2). The halogen groups of the monomers were removed by thermal activation on the Au surface to form biradical species, which subsequently underwent radical coupling reactions to form covalent C−C bonds between each monomer, yielding a chevron-type polyphenylene precursor. Finally, the polyphenylene precursor was annealed to a higher temperature of 450 °C to establish an extended fully aromatic system, where the surface-assisted intramolecular cyclodehydrogenation afforded the structurally defined chevron-type GNRs (Figure 1a). In contrast to the UHV[13] and the three-zone low-pressure CVD[28] processes reported before, a two-zone system and ambient pressure were used in our synthesis, for the first time demonstrating that the GNRs can be fabricated efficiently even under such readily available conditions. The results also proved that the surface-assisted polymerization and cyclodehydrogenation reactions for the GNR synthesis are pressure-independent, from UHV to ambient pressure. The CVD growth was carried out under a mixture of Ar and H_2, which is essential to suppress the oxidation of the resulting GNRs, as revealed by HREELS and XPS (*vide infra*). This CVD method can be further applied to different monomers, enabling ambient-pressure synthesis of heteroatom-doped GNRs as well as GNR heterojunctions (*vide infra*).

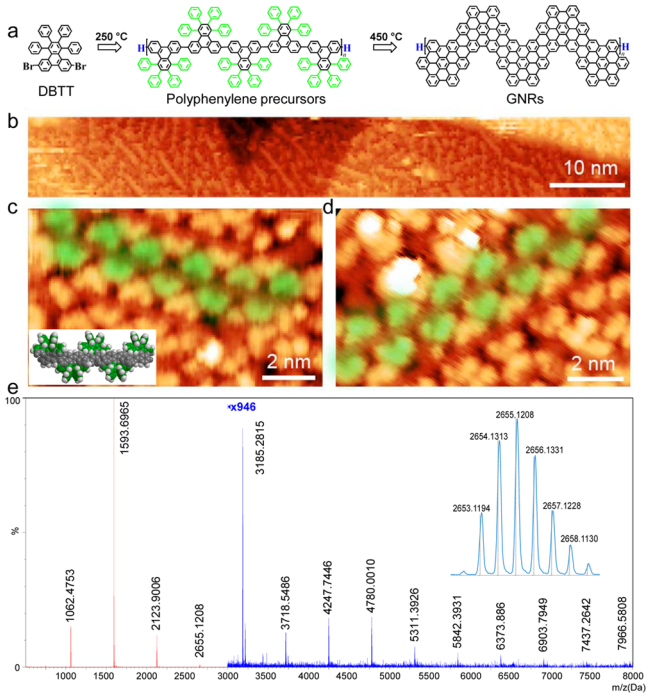

Figure 1. CVD growth of chevron-type GNRs and characterization of the intermediate polyphenylene precursors. (a) CVD reaction scheme to chevron-type GNRs. (b) 5 K UHV STM topography of the GNR polyphenylene precursors on Au/mica. (c,d) Zoom-ins highlighting undecameric and dodecameric polymer sections, where the tetraphenyl substitutions are marked in green (as they are in the structure model in the inset of (c) and in (a)). Contamination adsorbed during ambient-pressure CVD (white protrusions) make high-resolution, long-range surveys challenging. V_t = 1 V, I_t = 100 pA. (e) Mass spectrum of chevron-type polyphenylene precursors before cyclodehydrogenation, with a regular sequence of peaks from dimer ($m/z \approx 1062$ Da) to pentadecamer ($m/z \approx 7966$ Da). Inset shows the isotopic distributions of the pentamer precursor, which agree well with the simulated results given in dotted lines.

DOI: 10.1021/jacs.6b10374
J. Am. Chem. Soc. 2016, 138, 15488−15496

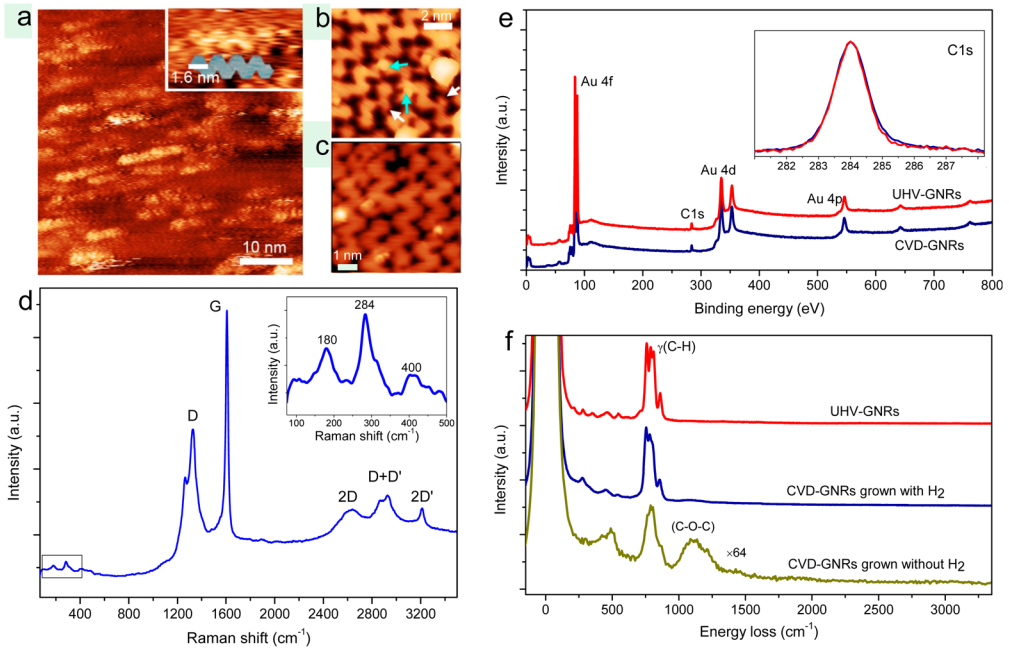

Figure 2. Microscopic and spectroscopic characterizations of chevron-type GNRs. (a) Ambient STM topography of the CVD-grown GNRs on Au/mica. A GNR model is also shown in the inset to scale. V_t = 450 mV, I_t = 15 pA. (b,c) 5 K UHV STM images depicting the chevron-type structure. Arrows in (b) highlight common GNR imperfections. V_t = 1 V, I_t = 50 pA. (d) Raman spectra of GNRs transferred on fused silica, measured at 532 nm; the inset is the magnified low-frequency mode (black oblong, bottom left). (e,f) XPS and HREELS spectra of the UHV-grown and CVD-grown GNRs. The HREELS spectrum of CVD-GNRs grown without H_2 is also shown in (f) for comparison. In the inset of (e), the C1s core-level spectra are presented.

Mass Spectrometry Characterization of the Intermediate Polyphenylene Precursors and GNRs. The polymerization reaction was first studied by high-resolution matrix-assisted laser desorption/ionization time-of-flight mass spectrometry (MALDI-TOF MS), which is a powerful method to assess the atomic composition of complex organic compounds.[35] For MALDI-TOF MS measurements, the {(2*E*)-2-methyl-3-[4-(2-methyl-2-propanyl)phenyl]-2-propen-1-ylidene}malononitrile (**DCTB**) matrix was sublimed on the as-deposited polyphenylene precursors on the Au/mica substrate. The MS spectrum exhibits regular patterns of polyphenylene precursors from dimer ($m/z \approx 1062$ Da) to pentadecamer ($m/z \approx 7966$ Da), in agreement with the expected mass values, which confirms the successful polymerization reaction (Figure 1e). The observed isotopic distribution is in perfect agreement with the simulated pattern, proving the precise chemical composition of the polyphenylene precursors (Figure 1e, inset). The intensities of these MS peaks decrease for longer polyphenylene precursors, and precursors larger than 15 repeating units, i.e., ∼12 nm in length were not observed. We have also successfully investigated the polymerization reaction in CVD growth of other GNRs, such as N = 7 armchair GNRs (7-AGNRs), using the high-resolution MS analysis method (Figure S3).

Understanding the nature of the GNR termini is important to reveal the factors limiting the length of GNRs.[29] There are mainly three plausible GNR termini, considering the steps of the CVD growth: radical, Br, and H passivation. By combining high-resolution SPM experiments with large-scale density functional theory simulations, Talirz et al. have demonstrated that the termini of GNRs grown under UHV conditions are passivated by hydrogen.[29] It was suggested that the H atoms come from premature cyclodehydrogenation in the polymerization step, which can directly compete with the polymerization reaction by forming a C−H bond at the radical termini. However, even with those atomically resolved STM analyses, the presence of the hydrogen atoms cannot be directly confirmed. Besides, no SPM investigation has been performed directly on the polyphenylene precursor to reveal its terminal structure in the polymerization reaction. Here, for the first time, we obtained stoichiometric information on the polyphenylene termini by MALDI-TOF MS analysis, as shown in Figures 1e and S4. No Br-terminated polyphenylene precursors can be detected in the samples polymerized at temperatures higher than 250 °C. Besides, the exact isotopic distribution of each polyphenylene does not match the radical termini but is in agreement with a H-passivated structure (Figure S4). These results indeed agree well with the SPM study on GNR termini.[29] However, no signal that can be attributed to premature cyclodehydrogenation of the precursor can be detected. The amount of premature cyclodehydrogenation might be too limited to be detected by MALDI-TOF MS even if it exists. The reported SPM analysis revealed that 15% of the GNR termini are methylene groups (H_2 passivation).[29] Nevertheless, MS analysis does not support such a termination for the polyphenylene precursors.

Whereas the polyphenylene precursors could be well characterized, the MALDI-TOF MS analysis of the resulting chevron-type GNRs on Au/mica substrates shows no meaningful signals. We suppose that the planar GNRs strongly interacting with the gold surface could not be effectively desorbed by MALDI.[17,36] When the GNRs were transferred onto a silicon wafer, some carbon fragments could be detected (Figure S5). Interestingly, all the observed fragments are even-numbered carbon clusters formed through destructive ablation of the GNRs by the laser irradiation in the MS system, which is remarkably similar to the LDI MS spectrum observed for graphene.[37]

DOI: 10.1021/jacs.6b10374
J. Am. Chem. Soc. 2016, 138, 15488−15496

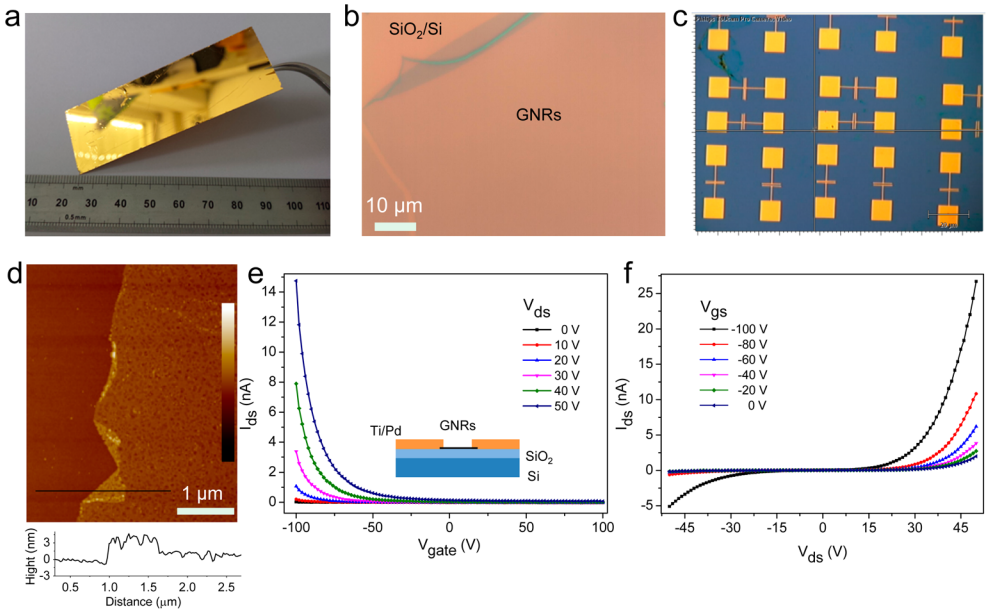

Figure 3. Transfer of CVD-grown chevron-type GNRs and microchannel FET device fabrication. (a) Photograph of a 25 × 75 mm^2 GNRs/Au/mica plate. (b) Optical microscope image of the GNR film transferred on SiO_2/Si substrate, showing the uniformity inside the film. The folding area can be found at the edge of the film. (c) Optical microscope image of the devices built on GNR film. (d) AFM topographical image of GNR film transferred on a silicon wafer. The *z*-scale ranges from −16.5 to 16.5 nm. The cross sectional high analysis is indicated along the black line. (e) Transfer curves of a typical GNR thin-film transistor measured at different V_{ds}. The results show that GNR transistors exhibit unipolar p-type behavior with on/off current ratio of >1000. The highest on/off ratio we measured is 6000. (f) I_{ds}−V_{ds} curves of the GNR transistors. The curves display highly nonlinear relationship, indicating a Schottky contact between electrodes and GNR channel.

UHV Characterizations of GNRs. Although the investigation of ambient-pressure samples under UHV conditions is generally challenging due to the atmospheric contaminants, UHV STM, XPS, and HREELS are key characterization methods for GNRs. Topographical STM surveys of the sample after the first polymerization step show chevron-type polyphenylene precursors (Figure 1b). High-resolution data reveal zigzag-shaped polymer chains, in good agreement with previous UHV-STM studies,[13] where the tetraphenyl substitutions marked in green in Figure 1a are tilted with respect to the surface, resulting in bright features in the STM images (Figure 1c,d). After the final cyclodehydrogenation step, a planar chevron-type structure of the resulting GNRs is identified in both ambient and UHV STM investigations (Figure 2a−c). A higher resolution UHV image reveals additional imperfections at the submolecular level. The white and cyan arrows in Figure 2b indicate common defects due to broken phenyl rings and randomly coupled GNRs, respectively. To be noted is that even the "atomically precise" GNRs made under UHV are not always 100% atomically precise, in terms of the curving and branching.[13] Recently, the coupling of several GNRs into complex junction structures has also been found in the UHV-grown GNRs and revealed by CO-functionalized atomic force microscopy (AFM) in atomic resolution.[38,39] These coupling junctions between GNRs may be important tools in the development of graphene-based circuitry and may facilitate the electronic device investigation on GNRs.[38] A large-scale survey was difficult to obtain due to adsorbed impurities from ambient-pressure conditions (bright white protrusions in Figures 1b−d and 2a−c), hindering quantitative statistical analysis of the GNR quality. Nevertheless, we would like to highlight that we can synthesize GNRs much faster and facilely under the CVD conditions with a significantly simpler setup, which can be easily scaled up for applications. We suggest that further preparation of the samples in clean-room conditions and vacuum packaging may improve the quality of GNRs and also facilitate the UHV STM characterization.

Instead, the quality of the CVD-grown chevron-type GNRs was further examined by comparing the XPS and HREELS spectra with those of a reference GNR sample, which was grown *in situ* under UHV conditions on a Au(111) single crystal[13] (Figures 2e,f). The overlayer coverage, as estimated from the intensity of the C1s peak relative to the Au 4f peak in the XPS spectrum, is very similar for both samples, corresponding to 0.5 ML for the UHV-grown GNRs and 0.6 ML for the CVD-grown GNRs (1 ML is defined as a single GNR layer with surface number density of 2.7 × 10^{15} at./cm^2, see the Supporting Information for details). The XPS survey spectra exhibit only the core-level peaks belonging to the GNRs and gold substrate. The C1s core-level spectrum of the CVD-grown GNRs consists of a single sharp component located at ∼284 eV binding energy, corresponding to the sp^2-bonded carbon, which well resembles that of the UHV-grown GNRs (Figure 2e). No Br components can be detected, indicating that Br atoms are completely desorbed from the gold surface. HREELS can precisely characterize the vibrational properties of the overlayer, serving as a powerful characterization method for GNR thin films especially when IR absorption is too weak for a reasonable analysis.[30,40] The HREELS spectra of the two samples are almost identical: both are indeed dominated by the out-of-plane CH mode manifold, located in the 700−850 cm^{-1} region, while the intensity of the in-plane CH stretching mode at 3063 cm^{-1} is almost negligible (Figure 2f). The manifold is built up by four main peaks located at 754, 782, 806, and 862 cm^{-1}, which are assignable to out-of-plane modes γ(C−H), characteristic of different molecular edge topologies (i.e., TRIO, DUO, and SOLO structures in refs 41 and 42.). It is important to notice that in both spectra the feature at ∼700 cm^{-1}, which is

DOI: 10.1021/jacs.6b10374
J. Am. Chem. Soc. 2016, 138, 15488−15496

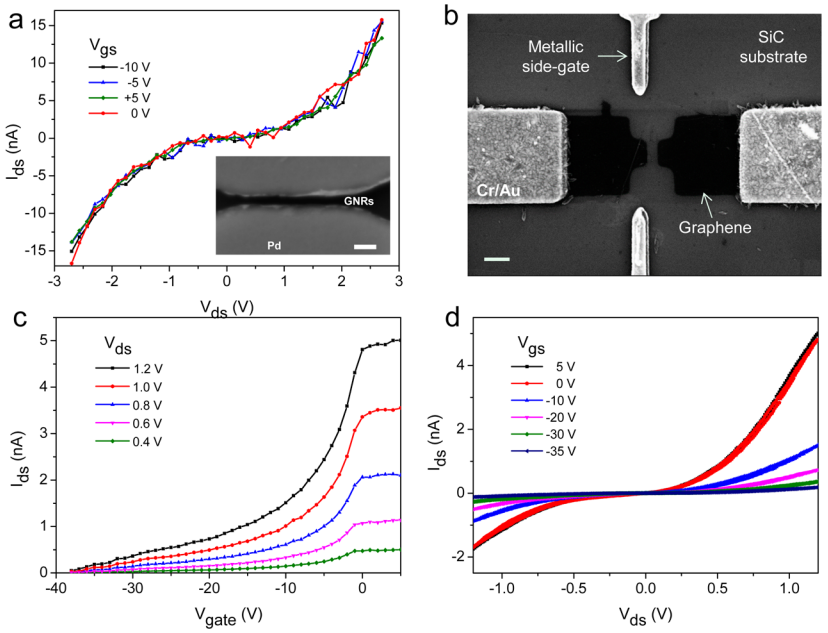

Figure 4. Electrical characteristics of nanochannel FET devices fabricated with CVD-grown chevron-type GNRs. (a) $I_{ds}-V_{ds}$ curves of the short-channel devices at various gate voltages. The inset shows the scanning electron micrograph (SEM) of a typical short-channel device with an electrode spacing of ~46 nm (scale bar, 100 nm). (b–d) Short-channel side-gate devices with graphene contacts: (b) SEM image of the device on SiC substrate (scale bar, 300 nm); (c) transfer curves of a typical GNR device with graphene electrodes, exhibiting an n-type conduction with high current on/off ratios; and (d) $I_{ds}-V_{ds}$ curves at different gate voltages. The nonlinear behavior of the $I_{ds}-V_{ds}$ curves indicates Schottky contacts with slightly asymmetric barriers.

attributed to the out-of-plane γ(C–H) mode of the monosubstituted benzene rings and is therefore present only for the monomer and polyphenylene precursors, is indeed barely visible.[30] This finding, together with the dominant intensity of out-of-plane modes relative to in-plane ones, proves that the reaction from the polyphenylene precursors to flat GNRs is completed.[30] The quality of the CVD-grown GNRs is also documented by the huge intensity of the elastic peak and the narrow width of the vibrational modes, which are comparable with those of the UHV-grown GNRs. The slight differences seen in the spectra might be caused by the atmospheric contaminants on the Au(111) surface under the ambient-pressure conditions. Besides, compared with UHV conditions, we have found that hydrogen is important for CVD growth of high-quality GNRs. Normally, the oxygen content in CVD is much larger than in the UHV system and is inevitable, leading to the considerable oxidation of the resulting GNRs, as evidenced by the HREELS analysis: The HREELS spectra of the CVD-GNRs grown without H_2 displays two extra broad features located at 440 and 1100 cm^{-1}, which may be attributed to C–O–C deformation and stretching modes (Figure 2f). Oxidation of the GNRs grown without H_2 was further corroborated by XPS, in which a much higher level of oxygen content was detected (see Figure S6 and the Supporting Information for details). High quality of the CVD-grown GNRs could be achieved only in the presence of H_2 in the growth, which can suppress the oxidation of the GNRs during the high-temperature annealing (Figure 2f). Therefore, combination of the high-resolution STM, HREELS, and XPS analyses proved that structurally defined GNRs can be synthesized by our CVD method in the presence of H_2, with high quality comparable to that of the UHV-grown GNRs.

Transfer of the GNRs and Their Raman and UV–Vis–NIR Spectroscopy Characterizations. The Raman spectra of the CVD-grown chevron-type GNRs excited by a 532 nm laser are presented in Figures 2d and S7, where the most intense peaks are at ~1330 and 1608 cm^{-1}, typically assigned to D and G bands, respectively.[43] Remarkably, sharp peaks of low-frequency modes can be observed at ~180, ~284, and ~403 cm^{-1}, which may be related to the specific GNR structure, like the width-specific radial breathing-like mode (RBLM),[13,19] indicating high uniformity of the chevron-type GNRs. The Raman spectrum of the CVD-grown 7-AGNRs demonstrates perfect agreement with that of the same GNR prepared under UHV conditions, including the RBLM at ~400 cm^{-1} and other smaller features, which further corroborates the highly defined structures of the CVD-grown GNRs (Figure S3).

Moreover, the quantity of GNRs and the size of the resulting films can be easily scaled up by using large Au/mica substrates, e.g., with an area of 25 × 75 mm^2, as shown in Figure 3a (essentially limited only by the furnace and tube dimensions), which is much larger than the reported small piece of GNRs formed by CVD (limited to a size of ~10 × 10 mm^2) using a similar size quartz tube.[28] After the CVD growth, the GNRs can be transferred onto other substrates with or without the assistance of poly(methyl methacrylate) (PMMA) (Schemes S2 and S3). The transferred GNR films possess a high uniformity over an area of square centimeters without any cracks based on the optical images and Raman mapping (Figures 3b and S7–S9). AFM of the GNRs transferred on silicon wafer reveals a thickness of ~0.7 nm (Figure 3d). The chevron-type GNR films have also been transferred layer by layer on fused silica for UV–vis–NIR absorption measurements (Figure S10). The spectrum exhibits absorption in the UV and visible regions, with an absorption maximum at ~450 nm. The optical bandgap of the GNR film was roughly estimated from the absorption onset at ~700 nm to be approximately 1.8 eV,[19,20] suggesting their potential for electronic device applications.

DOI: 10.1021/jacs.6b10374
J. Am. Chem. Soc. 2016, 138, 15488–15496

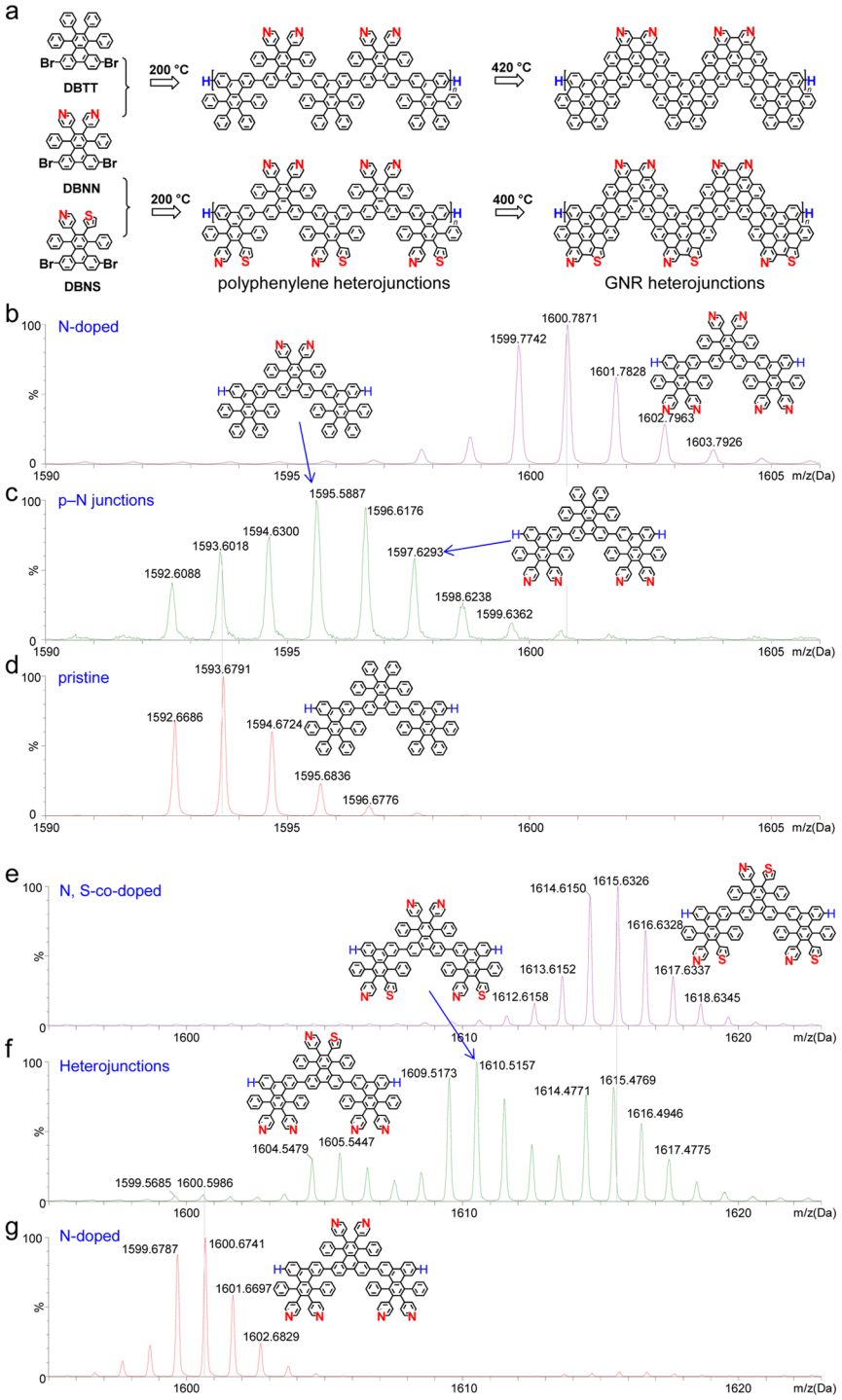

Figure 5. Heteroatom doping and heterojunctions of polyphenylene precursors and GNRs. (a) CVD reaction scheme to GNR heterojunctions by co-sublimation of **DBTT**/**DBNN** and **DBNS**/**DBNN**. (b–d) Isotopic analysis of the N-doped (b) and pristine (d) polyphenylene trimers and their co-deposited p-N polyphenylene heterojunctions (c) by high-resolution MALDI-TOF MS. (e–g) Isotopic analysis of the N,S-co-doped (e) and N-doped polyphenylene trimers (g) and their co-deposited polyphenylene heterojunctions (f) by high-resolution MALDI-TOF MS.

Electronic Properties of GNR-Based Three-Terminal FET Devices. Based on the successful transfer of chevron-type GNR films on any desired substrates, we have fabricated three-terminal FET devices using GNRs as the channel material, to study their charge transport properties. The first set of devices was fabricated from chevron-type GNR films transferred on a silicon wafer, where Pd/Ti (50 nm/1 nm) electrodes were patterned as the contact metals using electron-beam lithography (EBL) (Figure 3c). The channel length was ∼1–2 μm (see Supporting Information for more details). As shown in Figures 3e,f and S11a, a large gate modulation to the source–drain current can be observed (current on/off ratio >1000). The GNR transistors exhibit a unipolar p-type conduction, as the source–drain current increases with increasingly negative gate voltages. The p-type conduction might be caused by doping via adatoms (e.g., oxygen from air), since the device measurements were carried out in ambient conditions.[44] The best-performing devices exhibit current on/off ratios of >6000,

DOI: 10.1021/jacs.6b10374
J. Am. Chem. Soc. 2016, 138, 15488–15496

which is significantly higher (more than 3 orders of magnitude) than the values reported so far for other "bottom-up"-synthesized GNR thin-film network transistors (with typical on/off ratio of ~2−5),[27,28,34] and even better than those of the devices made from UHV-GNRs with an ultra-narrow channel.[44] Figure 3f shows $I_{ds}-V_{ds}$ curves of a typical GNR transistor. The nonlinear nature of the curves at small bias regimes suggests Schottky-contact behavior. This observation is understandable because our GNRs are very narrow and possess a large bandgap. Since the GNR devices reveal p-type conduction in air, the use of high work function contact materials, such as MoO_{3-x},[45] may offer better contacts to the valence band of GNRs and deliver better device performance.

Alternatively, reducing the channel length may also improve the device performance, as the additional resistance between adjacent ribbons is reduced or can be completely avoided. This has been tested in an additional set of devices where the Pd electrode was in direct contact with the GNR films and the spacing between the electrodes was smaller than 50 nm (Figure 4a). Because of the drastically reduced active channel length, the same level of current flow can be achieved at 1 order of magnitude lower source−drain voltages. However, in that case the influence of the gate voltage is drastically reduced, which may be attributed to the screening effect of the metal electrodes on the electric field from the gate. Therefore, either a thinner insulating barrier layer or a better source−drain electrode material would be needed to retain the FET functionality in the short-channel devices. For this purpose, and by taking advantage of the facile transfer process of our GNRs, we realized another type of three-terminal FET device by direct transfer of the chevron-type GNRs on prefabricated graphene electrodes, i.e., a graphene device where the channel has been opened with a gap of approximately 100 nm by EBL and oxygen plasma etching (see Figure 4b and the Supporting Information for details). Relatively thick graphene (average 10 layers) on the C-face of SiC is chosen as the electrode material, which displays almost no gate dependence and is expected to show limited screening of the gate potential compared to metal electrodes. The electrical characteristics of the resulting devices are presented in Figure 4c,d (see Figures S11−S13 and the Supporting Information for more details). The contact resistance is greatly reduced with respect to the long-channel metal electrodes, due to the shorter channel distance and a superior GNR/graphene interface. An evident transistor effect (current vs side-gate voltage) can be observed with a current on/off ratio of >100, limited only by the maximum applicable gate voltage. Improvement of the channel−gate coupling, for instance by employing a top gate with a thin high-*k* dielectric, is expected to further enhance the device performance. Interestingly, contrary to the p-type conduction observed in the long-channel devices, the devices based on graphene electrodes show an n-type conduction, which was previously found also for the UHV-GNR device.[44] The $I_{ds}-V_{ds}$ curves in Figure 4d remain nonlinear, indicating the presence of a Schottky-type contact also in these devices. We suggest that the performance of these GNR devices can be further improved by using hBN as its support. Moreover, development of wider GNRs with smaller bandgaps and growth of longer GNRs through optimization of the CVD process may further reduce the Schottky barriers and contact resistance for a better electrical connection to electrodes.

Heteroatom-Doped GNRs and GNR Heterojunctions. The "bottom-up" CVD procedure can be a general strategy for fabricating a broad class of GNRs and their hybrids with engineered structures and properties based on the selection of suitable monomers. As an example, we have demonstrated the CVD growth of heteroatom-doped chevron-type GNRs, which is a promising way to modify the electronic structures of GNRs.[14,30] By using the nitrogen- and sulfur-containing monomers 4,4′-(6,11-dibromo-1,4-diphenyltriphenylene-2,3-diyl)dipyridine (**DBNN**) and 4-(6,11-dibromo-1,4-diphenyl-3-(thien-3-yl)triphenylen-2-yl)pyridine (**DBNS** (Figure 5 and Scheme S1) as precursors, N-doped and N,S-co-doped chevron-type GNRs can be grown in the CVD system, respectively (Scheme S4). High-resolution MALDI-TOF MS analysis clearly validates the polymerization of the corresponding dehalogenated biradical intermediates, forming N-substituted and N,S-co-substituted polyphenylene precursors (Figures 5b,e, S14, and S15). Contrary to symmetric monomer **DBNN**, monomer **DBNS** has an asymmetric structure with both pyridyl and thienyl groups. Therefore, it must be noted that the resulting N,S-co-substituted polyphenylene precursors always contain regioisomeric segments, depending on the head-to-head or head-to-tail coupling, which can only be differentiated by atomic-resolution SPM. The successful cyclodehydrogenation of these precursors into the N-doped and N,S-co-doped GNRs is corroborated by Raman spectroscopy (Figure S16). The observation of intense Raman spectra with the sharp G peak located at ~1608 cm^{-1} and D peak located at ~1,330 cm^{-1} validated the successful "graphitization" of the polymer precursors into GNR structures. We have also performed XPS and HREELS analyses of the N-doped and N,S-co-doped GNRs grown by our CVD method (see Figures S17 and S18 and the Supporting Information for details).

We further fabricated GNR heterojunctions in the CVD system by co-sublimation of different kinds of structurally complementary monomers. Figure 5a illustrates the strategy for fabricating a p-N-GNR heterojunctions with seamlessly connected segments of pristine (p) and N-doped (N) GNRs.[14] The monomer **DBTT** and its N-substituted equivalent **DBNN** were co-deposited on a Au/mica substrate kept at 200 °C, resulting in polyphenylene heterojunctions, which could be directly identified by the MS analysis (Figures 5a,c and S19 and Scheme S4). The deposited radical intermediates of the two monomers distribute randomly and uniformly on the gold surface.[15] Therefore, the building blocks in the hybrid polyphenylene precursors are mixed and fused in a random sequence during the polymerization, exhibiting a statistical distribution from pure segments of each monomer unit to their combinations with different ratio. For example, the isotopic distributions of the resulted trimeric polyphenylene precursors exhibit four kinds of trimer structures, with the ratio of the two monomer units varying from 3/0, 2/1, 1/2, to 0/3, where the middle two structures are corresponding to the polyphenylene heterojunctions (Figure 5c). Moreover, the CVD method allows for the synthesis of polyphenylene heterojunctions with various chemical compositions simply by using different monomers. For example, heterojunctions of N-substituted and N,S-co-substituted polyphenylenes can be fabricated by combining the N-substituted and N,S-co-substituted monomers (**DBNN** and **DBNS**), which have been unambiguously identified by high-resolution MS analysis (Figures 5f and S20). These results mark the high versatility of the CVD process and the great effectiveness of this direct MS analysis method for investigating the GNR growth process. All these polyphenylene heterojunctions can be converted to

DOI: 10.1021/jacs.6b10374
J. Am. Chem. Soc. 2016, 138, 15488−15496

GNR heterojunctions similarly by cyclodehydrogenation upon further thermal annealing at 400−420 °C, as verified by Raman spectroscopic analyses (Figure S16).

CONCLUSION

In summary, the low-cost CVD method has enabled the large-scale "bottom-up" growth of structurally defined pristine GNRs and selectively N-doped and N,S-co-doped GNRs as well as their heterojunctions at ambient pressure, which can be an excellent complement to the more elaborate UHV method. Raman, HREELS, XPS, and STM analyses manifested the high quality of the CVD-grown GNRs, well comparable to those grown under UHV conditions. Mass spectrometry analysis on the surface can serve as a quick and powerful method to investigate the precise chemical structures of various GNR precursors as well as other surface-bound molecular materials. Further studies might also provide insight into the reaction mechanisms of the surface-based polymerization and cyclodehydrogenation. Large-area GNR films can be readily transferred onto arbitrary substrates, where preliminary micro- as well as nanoscale transistor devices could be fabricated, demonstrating unprecedentedly strong gate modulation for the "bottom-up" GNRs. Furthermore, our large-scale synthesis process can be readily applied to other designed monomers for preparing GNRs with engineered topographic and chemical structures, which is expected to provide practical solutions to the current challenges in graphene-based nanoelectronic, optoelectronic, and photonic devices.

EXPERIMENTAL SECTION

CVD Growth of GNRs. Home-made and commercially available (Phasis, Switzerland and Georg Albert, Germany) 200 nm Au thin films epitaxially grown on mica were used as substrates for GNR growth. They were cut into pieces with sizes from 10 × 10 to 25 × 75 mm^2 and placed in a quartz tube of outer diameter 35 mm and inner diameter 33 mm in a horizontal tube furnace (Nabertherm, RT 80-250/11S). Precursor monomers (for details on the synthesis, see the Supporting Information) were loaded upstream of the Au/mica substrates and sublimed at 250−325 °C onto the Au/mica surface using a heating belt (Thermocoax Isopad S20). The Au/mica substrates were heated and maintained at 200−250 °C under gas flow of Ar (500 sccm) and H_2 (100 sccm) during monomer sublimation for 5−30 min to induce dehalogenation and radical addition reaction. After deposition, the samples were postannealed at 400−450 °C for 15 min to convert the polyphenylene precursors into GNRs by cyclodehydrogenation. For fabrication of the heterojunctions, the two precursor species were evaporated together onto a Au/mica substrate held at 200 °C, which was subsequently annealed to 400−420 °C. To study the oxidation of the GNRs, only 500 sccm of Ar was used in the growth without H_2, the pressure was ∼0.7 mbar by a mechanical rotary pump (capable of low pressure down to $<10^{-4}$ mbar).

Transfer of GNRs. As-grown GNRs/Au/mica substrates were placed on a surface of hydrofluoric acid (HF, 40 wt%) solution, which etched away the mica and made the Au film with GNRs float on the surface of the HF solution. After being washed with ultra-pure water, the GNRs/Au films were transferred to a new insulated substrate and dried at 100 °C for 10 min. Finally, the Au films were etched away by gold etchant (Sigma-Aldrich), leaving only the GNR films on the new substrate. When transferring GNR films with large areas, spin-coated PMMA thin films were used as a mechanical support before etching with HF to avoid breaking the GNR films. The PMMA was washed away by hot acetone in the last step (Schemes S2 and S3).

ASSOCIATED CONTENT

Supporting Information

The Supporting Information is available free of charge on the ACS Publications website at DOI: 10.1021/jacs.6b10374.

Experimental details and characterization data, MALDI-TOF MS, Raman spectra, UV−vis−NIR spectra, and more analysis on XPS and HREELS spectra of the GNRs and their FET devices, including Figures S1−S20 and Schemes S1−S4 (PDF)

X-ray crystallographic data for **DBNS** (CIF)

AUTHOR INFORMATION

Corresponding Authors

*xinliang.feng@tu-dresden.de

*muellen@mpip-mainz.mpg.de

ORCID

Wen Zhang: 0000-0001-8847-1664

Florian Klappenberger: 0000-0002-2877-6105

Andrea Candini: 0000-0003-3909-473X

Notes

The authors declare no competing financial interest.

ACKNOWLEDGMENTS

This work was supported by the European Research Council grant on NANOGRAPH and MolArt, DFG Priority Program SPP 1459, MIUR FIR grant RBFR13YKWX and project PRIN-GRAF 20105ZZTSE_008, Graphene Flagship (No. CNECT-ICT-604391), European Union Projects UPGRADE and MoQuaS (contract N.610449), and the Office of Naval Research BRC Program. The authors thank Dr. Roberto Biagi and Valdis Corradini (CNR-NANO, Istituto Nanoscienze) for useful discussions, F. Carillo and P. Pingue (Laboratorio NEST, Scuola Normale Superiore, Pisa) for support on the sample fabrication, and Dr. Dieter Schollmeyer (Institute for Organic Chemistry, Johannes Gutenberg University Mainz) for single-crystal X-ray structural analysis of the monomer **DBNS**. X.Y.W. is grateful for the fellowship from the Alexander von Humboldt Foundation.

REFERENCES

(1) Novoselov, K. S.; Geim, A. K.; Morozov, S. V.; Jiang, D.; Zhang, Y.; Dubonos, S. V.; Grigorieva, I. V.; Firsov, A. A. *Science* **2004**, *306*, 666−669.

(2) Geim, A. K. *Science* **2009**, *324*, 1530−1534.

(3) Geim, A. K.; Novoselov, K. S. *Nat. Mater.* **2007**, *6*, 183−191.

(4) Kotov, V. N.; Uchoa, B.; Pereira, V. M.; Guinea, F.; Castro Neto, A. H. *Rev. Mod. Phys.* **2012**, *84*, 1067−1125.

(5) Castro Neto, A. H.; Guinea, F.; Peres, N. M. R.; Novoselov, K. S.; Geim, A. K. *Rev. Mod. Phys.* **2009**, *81*, 109−162.

(6) Yang, L.; Park, C. H.; Son, Y. W.; Cohen, M. L.; Louie, S. G. *Phys. Rev. Lett.* **2007**, *99*, 186801.

(7) Barone, V.; Hod, O.; Scuseria, G. E. *Nano Lett.* **2006**, *6*, 2748−2754.

(8) Palma, C.-A.; Awasthi, M.; Hernandez, Y.; Feng, X.; Müllen, K.; Niehaus, T. A.; Barth, J. V. *J. Phys. Chem. Lett.* **2015**, *6*, 3228−3235.

(9) Chen, Z.; Lin, Y.-M.; Rooks, M. J.; Avouris, P. *Phys. E* **2007**, *40*, 228−232.

(10) Han, M. Y.; Ozyilmaz, B.; Zhang, Y.; Kim, P. *Phys. Rev. Lett.* **2007**, *98*, 206805.

(11) Jiao, L. Y.; Zhang, L.; Wang, X. R.; Diankov, G.; Dai, H. J. *Nature* **2009**, *458*, 877−880.

(12) Kosynkin, D. V.; Higginbotham, A. L.; Sinitskii, A.; Lomeda, J. R.; Dimiev, A.; Price, B. K.; Tour, J. M. *Nature* **2009**, *458*, 872−876.

DOI: 10.1021/jacs.6b10374
J. Am. Chem. Soc. 2016, 138, 15488−15496

(13) Cai, J. M.; Ruffieux, P.; Jaafar, R.; Bieri, M.; Braun, T.; Blankenburg, S.; Muoth, M.; Seitsonen, A. P.; Saleh, M.; Feng, X. L.; Müllen, K.; Fasel, R. *Nature* **2010**, *466*, 470−473.
(14) Cai, J. M.; Pignedoli, C. A.; Talirz, L.; Ruffieux, P.; Söde, H.; Liang, L. B.; Meunier, V.; Berger, R.; Li, R. J.; Feng, X. L.; Müllen, K.; Fasel, R. *Nat. Nanotechnol.* **2014**, *9*, 896−900.
(15) Chen, Y. C.; Cao, T.; Chen, C.; Pedramrazi, Z.; Haberer, D.; de Oteyza, D. G.; Fischer, F. R.; Louie, S. G.; Crommie, M. F. *Nat. Nanotechnol.* **2015**, *10*, 156−160.
(16) Dössel, L.; Gherghel, L.; Feng, X.; Müllen, K. *Angew. Chem., Int. Ed.* **2011**, *50*, 2540−2543.
(17) Schwab, M. G.; Narita, A.; Hernandez, Y.; Balandina, T.; Mali, K. S.; De Feyter, S.; Feng, X.; Müllen, K. *J. Am. Chem. Soc.* **2012**, *134*, 18169−18172.
(18) Yang, X.; Dou, X.; Rouhanipour, A.; Zhi, L.; Rader, H. J.; Müllen, K. *J. Am. Chem. Soc.* **2008**, *130*, 4216−4217.
(19) Narita, A.; Feng, X.; Hernandez, Y.; Jensen, S. A.; Bonn, M.; Yang, H.; Verzhbitskiy, I. A.; Casiraghi, C.; Hansen, M. R.; Koch, A. H.; Fytas, G.; Ivasenko, O.; Li, B.; Mali, K. S.; Balandina, T.; Mahesh, S.; De Feyter, S.; Müllen, K. *Nat. Chem.* **2014**, *6*, 126−132.
(20) Vo, T. H.; Shekhirev, M.; Kunkel, D. A.; Morton, M. D.; Berglund, E.; Kong, L.; Wilson, P. M.; Dowben, P. A.; Enders, A.; Sinitskii, A. *Nat. Commun.* **2014**, *5*, 3189.
(21) Narita, A.; Verzhbitskiy, I. A.; Frederickx, W.; Mali, K. S.; Jensen, S. A.; Hansen, M. R.; Bonn, M.; De Feyter, S.; Casiraghi, C.; Feng, X.; Müllen, K. *ACS Nano* **2014**, *8*, 11622−11630.
(22) Chen, L.; Hernandez, Y.; Feng, X.; Müllen, K. *Angew. Chem., Int. Ed.* **2012**, *51*, 7640−7654.
(23) Narita, A.; Wang, X. Y.; Feng, X. L.; Müllen, K. *Chem. Soc. Rev.* **2015**, *44*, 6616−6643.
(24) Lee, S. J.; Kim, J.-Y.; Kim, H. P.; Kim, D.; da Silva, W. J.; Schneider, F. K.; Mohd Yusoff, A. R. b.; Jang, J. *Chem. Commun.* **2015**, *51*, 9185−9188.
(25) Osella, S.; Narita, A.; Schwab, M. G.; Hernandez, Y.; Feng, X.; Müllen, K.; Beljonne, D. *ACS Nano* **2012**, *6*, 5539−5548.
(26) Bonaccorso, F.; Sun, Z.; Hasan, T.; Ferrari, A. C. *Nat. Photonics* **2010**, *4*, 611−622.
(27) Abbas, A. N.; Liu, G.; Narita, A.; Orosco, M.; Feng, X. L.; Müllen, K.; Zhou, C. W. *J. Am. Chem. Soc.* **2014**, *136*, 7555−7558.
(28) Sakaguchi, H.; Kawagoe, Y.; Hirano, Y.; Iruka, T.; Yano, M.; Nakae, T. *Adv. Mater.* **2014**, *26*, 4134−4138.
(29) Talirz, L.; Söde, H.; Cai, J.; Ruffieux, P.; Blankenburg, S.; Jafaar, R.; Berger, R.; Feng, X.; Müllen, K.; Passerone, D.; Fasel, R.; Pignedoli, C. A. *J. Am. Chem. Soc.* **2013**, *135*, 2060−2063.
(30) Bronner, C.; Stremlau, S.; Gille, M.; Brausse, F.; Haase, A.; Hecht, S.; Tegeder, P. *Angew. Chem., Int. Ed.* **2013**, *52*, 4422−4425.
(31) Zhang, Y.; Zhang, Y. F.; Li, G.; Lu, J. C.; Lin, X.; Du, S. X.; Berger, R.; Feng, X. L.; Müllen, K.; Gao, H. J. *Appl. Phys. Lett.* **2014**, *105*, 023101.
(32) Batra, A.; Cvetko, D.; Kladnik, G.; Adak, O.; Cardoso, C.; Ferretti, A.; Prezzi, D.; Molinari, E.; Morgante, A.; Venkataraman, L. *Chem. Sci.* **2014**, *5*, 4419−4423.
(33) Vo, T. H.; Shekhirev, M.; Kunkel, D. A.; Orange, F.; Guinel, M. J. F.; Enders, A.; Sinitskii, A. *Chem. Commun.* **2014**, *50*, 4172−4174.
(34) Zschieschang, U.; Klauk, H.; Mueller, I. B.; Strudwick, A. J.; Hintermann, T.; Schwab, M. G.; Narita, A.; Feng, X. L.; Müllen, K.; Weitz, R. T. *Adv. Electron. Mater.* **2015**, *1*, 1400010.
(35) Hillenkamp, F.; Peter-Katalinic, J. *MALDI MS: a practical guide to instrumentation, methods and applications*; John Wiley & Sons: New York, 2013.
(36) Palma, C. A.; Diller, K.; Berger, R.; Welle, A.; Björk, J.; Cabellos, J. L.; Mowbray, D. J.; Papageorgiou, A. C.; Ivleva, N. P.; Matich, S.; Margapoti, E.; Niessner, R.; Menges, B.; Reichert, J.; Feng, X.; Rader, H. J.; Klappenberger, F.; Rubio, A.; Müllen, K.; Barth, J. V. *J. Am. Chem. Soc.* **2014**, *136*, 4651−4658.
(37) Kong, X.; Huang, Y.; Chen, Y. *J. Mass Spectrom.* **2012**, *47*, 523−528.
(38) Dienel, T.; Kawai, S.; Söde, H.; Feng, X.; Müllen, K.; Ruffieux, P.; Fasel, R.; Gröning, O. *Nano Lett.* **2015**, *15*, 5185−5190.
(39) Kawai, S.; Saito, S.; Osumi, S.; Yamaguchi, S.; Foster, A. S.; Spijker, P.; Meyer, E. *Nat. Commun.* **2015**, *6*, 8098.
(40) Bronner, C.; Leyssner, F.; Stremlau, S.; Utecht, M.; Saalfrank, P.; Klamroth, T.; Tegeder, P. *Phys. Rev. B: Condens. Matter Mater. Phys.* **2012**, *86*, 085444.
(41) Centrone, A.; Brambilla, L.; Renouard, T.; Gherghel, L.; Mathis, C.; Müllen, K.; Zerbi, G. *Carbon* **2005**, *43*, 1593−1609.
(42) Tommasini, M.; Lucotti, A.; Alfè, M.; Ciajolo, A.; Zerbi, G. *Spectrochim. Acta, Part A* **2016**, *152*, 134−148.
(43) Ferrari, A. C.; Meyer, J. C.; Scardaci, V.; Casiraghi, C.; Lazzeri, M.; Mauri, F.; Piscanec, S.; Jiang, D.; Novoselov, K. S.; Roth, S.; Geim, A. K. *Phys. Rev. Lett.* **2006**, *97*, 187401.
(44) Bennett, P. B.; Pedramrazi, Z.; Madani, A.; Chen, Y. C.; de Oteyza, D. G.; Chen, C.; Fischer, F. R.; Crommie, M. F.; Bokor, J. *Appl. Phys. Lett.* **2013**, *103*, 253114.
(45) Chuang, S.; Battaglia, C.; Azcatl, A.; McDonnell, S.; Kang, J. S.; Yin, X. T.; Tosun, M.; Kapadia, R.; Fang, H.; Wallace, R. M.; Javey, A. *Nano Lett.* **2014**, *14*, 1337−1342.

DOI: 10.1021/jacs.6b10374
J. Am. Chem. Soc. 2016, 138, 15488−15496